WILEY-VCH

DOI: 10.1002/ (adsu.201700113)
Article type: (Full Paper)

Highly-permeable Oligo (ethylene oxide)-co-Poly(dimethylsiloxane) Membranes for Carbon Dioxide Separation

*Tao Hong, Sophia Lai, Shannon M. Mahurin, Peng-Fei Cao, Dmitry N. Voylov, Harry M. Meyer, III, Christopher B. Jacobs, Jan-Michael Y. Carrillo, Alexander Kisliuk, Ilia N. Ivanov, De-en Jiang, Brian K. Long, Jimmy W. Mays, Alexei P. Sokolov, Tomonori Saito**

Dr. T. Hong, Dr. D. N. Voylov, Prof. B. K. Long, Prof. J. W. Mays, Prof. A. P. Sokolov
Department of Chemistry, University of Tennessee, Knoxville, Tennessee 37996, USA

S. Lai, Dr. S. M. Mahurin, Dr. P. Cao, Dr. A. Kisliuk, Prof. J. W. Mays, Prof. A. P. Sokolov, Dr. T. Saito
Chemical Sciences Division, Oak Ridge National Laboratory, Oak Ridge, Tennessee 37831, USA

E-mail: saitot@ornl.gov

Dr. H. M. Meyer, III
Materials Science and Technology Division, Oak Ridge National Laboratory, Oak Ridge, Tennessee 37831, USA

Dr. C. B. Jacobs, Dr. J. Y. Carrillo, Dr. I. N. Ivanov
Center for Nanophase Materials Sciences, Oak Ridge National Laboratories, Oak Ridge, Tennessee 37831, USA

Prof. D. Jiang
Department of Chemistry, University of California, Riverside, Riverside, California 92521, USA

Keywords: membrane gas separation, CO_2-philic, oligo (ethylene oxide), polydimethylsiloxane, high permeability

A series of cross-linked, free-standing oligo (ethylene oxide)-co-(polydimethylsiloxane-norbornene) (oligo (EO)-PDMSPNB) membranes with varied composition is synthesized *via in-situ* ring-opening metathesis polymerization. These membranes show remarkably high CO_2 permeabilities (3400 Barrer) and their separation performance approaches the Robeson Upper Bound. The excellent permeability of these copolymer membranes provides great potential for real world applications where enormous volumes of gases must be separated. The gas transport properties of these films are found to be directly proportional to oligo (EO) content incorporation, which stems from the increased solubility selectivity change within the copolymer matrix. This work provides a systematic study of how gas separation performance in rubbery membranes can be enhanced by tuning the CO_2-philicity of their constituent monomeric subunits.

1. Introduction

Climate change over the last few decades has been widely discussed and excessive greenhouse gas emissions, especially carbon dioxide (CO_2), are considered to be key contributors.[1-3] Various technologies are under development to mitigate these CO_2 emissions, and among them membrane separation is highlighted as one of the most promising approaches for sustainable development. This is in part due to the significantly reduced energy consumption associated with membrane-based separations as compared to other conventional separation techniques.[4-5] In order to deploy a membrane-based separation technology in post-combustion flue gas treatment, high-performance membrane materials, i.e. high permeability and selectivity, are required.[6-7] Due to the limited pressure difference, cost reductions associated with increasing CO_2/N_2 selectivity reach a plateau at selectivities exceeding 30. [8] The recent review article published in *Science* by Freeman *et al.* also emphasized the

importance of high gas permeability/permeance.[9] Membranes with ever increasing permeability/permeance are projected to provide continuous cost reduction due to their ability to treat larger volumes of flue gas.

Traditionally, many gas separations were accomplished using what is known as "size-sieving" membranes. However, the efficiency of CO_2/N_2 separations when using this traditional size-sieving approach has strong limitations due to the similar kinetic diameters of the two primary gases to be separated, primarily CO_2 and N_2 (kinetic diameters are CO_2~3.30 Å and N_2~ 3.64 Å).[10] On the other hand, the enhancement of CO_2/N_2 solubility selectivity *via* the introduction of CO_2-philic groups into the polymer matrix is known to increase CO_2/N_2 selectivity; however, the limitation of this approach is not known. A great deal of research has focused on poly(ethylene oxide) (PEO) functionality, which shows high affinity for quadrupolar CO_2 molecules[11-17]. As estimated by Lin and Freeman, the CO_2/N_2 selectivity in amorphous PEO could reach 48, which exceeds the practical CO_2/N_2 selectivity requirement for flue gas treatment.[18] However, as compared to some highly permeable polymers, e.g. poly (1-trimethylsilyl-1-propyne), [19-22] polymers of intrinsic microporosity,[23-26] and poly(dimethylsiloxane) (PDMS),[27-28] PEO shows one or two orders of magnitude lower gas permeability. For example, PDMS, a typical highly permeable rubbery polymer, exhibits about 25 times higher CO_2 permeability than that of amorphous PEO, which primarily originates from significantly different gas diffusivity between those two.[18, 27] Moreover, the undesirable semi-crystalline nature of PEO additionally reduces gas diffusivity, leading to further loss of gas permeability. Generally, high molecular weight PEO exhibits better mechanical properties, but also displays higher crystallinity and lower gas permeability. Low molecular weight PEO has lower crystallinity and better gas transport properties, but exists in liquid form and cannot be directly used as a free-standing gas separation membrane. Due to the inherently low permeability of PEO, regardless of molecular weight, the design of free standing PEO-containing membranes having high gas permeability presents a significant

challenge. In recent years, researchers have reported a variety of modifications of PEO-containing materials, aiming to achieve better gas transport properties as well as acceptable mechanical strength.[16-17, 29-31]

We hypothesized that a material combining the advantages of both PDMS and PEO could offer great advantages for high-performance gas separation membranes due to PDMS's high permeability and PEO's high selectivity for CO_2 separation. The majority of current studies focused on polymer blends and composite membranes which possess permeabilities typically below 700 Barrer. From a fundamental material design aspect toward achieving a breakthrough of material property, the development of high-performing/highly-permeable polymers is imperative for further advancement of the CO_2 separation technology and thus for the reduction of the carbon capture cost in the future.

Our recent simulation work revealed that the oligo (EO) functionality exhibits strong affinity with CO_2 molecules[32]; however, it remains challenging to fabricate a free-standing oligo (EO) membrane. In our previous studies, we reported *in-situ* ring-opening metathesis polymerization (ROMP) of lightly-cross-linked polydimethylsiloxane-norbornene (XLPDMSPNB) membranes,[28, 33] which offered a feasible approach to synthesize norbornyl-based membranes. Herein, we apply the advantage of the ROMP technique and report for the first time the successful copolymerization to produce free-standing oligo (EO)-PDMSPNB materials with enhanced CO_2/N_2 separation performance. These membranes combine the advantages of high PDMS permeability and strong oligo (EO)-CO_2 interactions. The utilization of oligo (EO) in the copolymer matrix prevents crystallinity to overcome the permeability loss, while still offering enhanced CO_2 solubility. The synthesized material results in one of the highest CO_2 permeabilities for PEO-containing membranes (3400 Barrer) and achieves performance that approaches the Robeson Upper Bound.

2. Results and Discussion

2.1. Membrane fabrication and properties

All membranes were formed *via in-situ* ROMP (**Scheme 1**) and showed a free-standing, transparent, homogeneous, and elastic nature. The compositions of oligo (EO)-PDMSPNB membranes were confirmed using FTIR (**Figure 1**). For the oligo (EO) moiety, the CH_2 scissoring and CH_2 asymmetric bending bands are observed at 1448 cm^{-1} and 1351 cm^{-1}, respectively.[34-36] The absorption band located at 1110 cm^{-1} for the C-O-C stretching mode is covered by Si-CH_3 symmetric deformation. For PDMS, the CH_3 asymmetric deformation is observed at 1408 cm^{-1}.[37] The systematic change of oligo (EO) and PDMS peaks can be observed in Figure 1(b). With increasing oligo (EO) feed ratio, the CH_2 scissoring and CH_2 asymmetric bending peaks show an increase relative to the CH_3 asymmetric deformation peaks of PDMS, indicating higher oligo (EO) content in the copolymer membranes.

The membrane composition is estimated by thermogravimetric analysis (TGA) and the results are shown in **Figure 2**. The data of starting material, NB-oligo (EO) and pure XLPDMSPNB membranes are shown in dashed curves. The oligo (EO)-PDMSPNB copolymers demonstrate good thermal stability and exhibit a two-step decomposition, indicating that the PDMS and oligo (EO) components have different thermal stabilities. With higher oligo (EO) composition, the decomposition process shows a slight shift toward lower temperature. It is observed that over 95% of NB-oligo (EO) is decomposed at 450 °C, while it is only ~5% for PDMS moiety. Based on previous studies, PDMS is typically stable until around 430 °C, while PEO is likely to be completely decomposed at this temperature.[38-39] Thus, in this study, the oligo (EO) compositions are estimated from the weight percentage at the 450 °C (see the vertical dashed line in Figure 2), which corresponds to the onset of PDMS decomposition. The results are summarized in Table 1, and the sample codes correspond to wt% of NB-oligo (EO) moiety

determined by TGA measurements. It can be noticed that the estimated NB-oligo (EO)/PDMS compositions are similar to the original feed ratio.

The tensile properties, e.g. Young's modulus(Et), ultimate tensile strength and elongation at break(ε), of oligo (EO)-PDMSPNB membranes were tested by dynamic mechanical analysis (DMA). The data are shown in **Figure S1** and **Table S1**. The obtained results agree well with the previously reported PDMS materials.[40-41] Due to the rubbery nature of oligo (EO)-PDMSPNB membranes, Young's modulus values ranged from 0.15 to 0.40 MPa, while the elongation is around 100-200%.

The differential scanning calorimetry (DSC) data for oligo (EO)-PDMSPNB membranes are shown in **Figure 3**, and the glass transition temperatures (T_g) are summarized in Table 1. The glass transition process for PDMS can be estimated from both the transition process in reversible heat flow curves (Figure 3 (a)) and the peak position in the derivative curves (Figure 3 (b)). The glass transition process for oligo (EO) segment is masked by the PDMS melting process and can only be seen from the derivative curves. The T_g values for both PDMS ($T_{g,1}$,-124 °C) and oligo (EO) ($T_{g,2}$, around -58°C) agree well with previously reported data.[42-43]

The presence of two T_g values suggests the occurrence of slight phase separation between the two chemical compositions. The morphology of the (oligo (EO)-PDMSPNB membrane was further investigated by small-angle X-ray scattering (SAXS). In **Figure S2**, the appearance of a broad peak at 0.02 $Å^{-1}$ confirmed the phase separation of the two polymer components. However, SAXS data also indicated the lack of any long-range order in their morphology due to the absence of any ordered multiple peaks and the presence of the very broad first diffraction peak.

For all measured samples, the crystallization and melting processes of PDMS are observed (Figure 3(a)). However, the PEO melting temperature is usually around 70 °C,[18, 44] which was not observed in DSC thermograms, indicating no measurable crystallization of oligo (EO)

segments. It is within our expectation that due to the use of oligo (EO) and the introduction of cross-linking, the crystallization is prevented in these membranes. The suppression of crystallization could well contribute to the improvement of gas diffusivity.

2.2. Gas transport property

Gas permeabilities and CO_2/N_2 selectivites of the oligo (EO)-PDMSPNB membranes are shown in **Figure 4** and summarized in Table 1. The gas permeability measurements are performed under varying pressures: 0.2atm, 0.5atm, 1.0 atm and 1.5 atm and 2.0 atm.

The gas permeability as a linear function of Δp can be written as:

$$P = P_0(1 + m\Delta P) \quad (1)$$

where P_0 is the permeability coefficient at Δp=0, the slope, m, characterizes the pressure dependence of permeability, and Δp is the pressure difference of upstream and downstream. Typically, the upstream pressure is much higher than the downstream pressure. Thus, Δp is replaced by upstream feed pressure.

The results in Figure 4 and Table 1 demonstrate that the gas permeability showed some, but very weak dependence on feed pressure. Compared with gas permeability obtained at high pressure, the P_0 values always showed less than 5% difference. Consider the possible experimental error during the measurements, we assume that the gas permeabilities are independent on feed pressure in oligo (EO)-PDMSPNB membranes. The pressure-independent gas separation performance of these membranes indicates great potential to be used in a variety of applications.

It can be noticed that both CO_2 and N_2 permeability follow a monotonous decreasing trend with higher oligo (EO) content in the membranes (Figure 4 (a) and (b)). When oligo (EO) content is low (18%), the gas permeability is still comparable to that of XLPDMSPNB.[28]

After 41% oligo (EO) is incorporated, the CO_2 permeability exhibits about a 65% decrease. This drop of gas permeability is likely due to the incorporation of oligo (EO) components, which provide relatively slow segmental motion/gas diffusion, as well as the use of oligo (EO) chains, which can form a more tightly cross-linked network, leading to further decrease of chain mobility/gas diffusivity. Moreover, the slight change of membrane density indicates the variation of chain packing efficiency/fractional free volume (FFV) in the membrane matrix. The higher oligo (EO) content membranes, which show slightly higher density, should possess decreased FFV, which could also contribute to the some decrease of gas diffusivity. Despite this, when compared to many previously reported PEO-containing membranes,[16-17, 30-31] our oligo (EO)-PDMSPNB membranes show about one order of magnitude higher CO_2 permeability. For CO_2/N_2 selectivity, it is observed that the selectivity of oligo (EO)-18 and oligo (EO)-24 are lower than that of PDMSPNB. Due to the use of short chain NB-oligo (EO), compared to PDMSPNB without oligo (EO), the cross-link density was significantly increased to enable the formation a free-standing film. The higher cross-link density leads to decreased gas selectivity, as was reported in our previous work.[28] However, by further increasing oligo (EO) content, the selectivity is enhanced (Table 1).

The improvement of CO_2/N_2 selectivity (Figure 4 (c)) relative to the XLPDMSPNB membranes reveals the great potential of oligo (EO)-PDMSPNB membranes for being applied in a practical flue gas treatment. When plotting the permeability data on a Robeson plot (Figure 4(d)), the highest performing sample (oligo (EO)-34) has achieved parameters very close to the upper bound, indicating its advanced performance as compared with other purely polymeric membranes. Furthermore, these high-performing, free-standing oligo (EO)-containing membranes can be used as is, or a gutter layer in addition to a selective layer in gas separation applications.

2.3. Gas sorption property

To further investigate the gas transport mechanism of oligo (EO)-PDMSPNB membranes, CO_2 sorption measurements were performed and the calculated solubility values are presented in **Figure S3** and **Table 2**. Generally, for most rubbery polymers, due to the low Langmuir sorption, their sorption behavior is well-described by Henry's law. However, due to the existence of norbornyl junctions, which serve as a glassy domain within the polymer matrix, the Henry's law fitting was slightly deviated. Thus, the dual-mode model is used to fit the sorption curves:[45]

$$C = k_D p + \frac{C'_H bp}{1 + bp} \quad (2)$$

where C is the equilibrium penetrant concentration in the polymer at pressure p, k_D is the Henry's law solubility parameter describing penetrant dissolution into the equilibrium densified polymer matrix, and C'_H is the Langmuir capacity parameter, which describes the sorption capacity of the nonequilibrium excess free volume characteristic of the glassy state. The Langmuir affinity parameter, b, is an equilibrium constant describing the affinity of a penetrant for a Langmuir site.

The fitting parameters are summarized in Table 2. For condensed rubbery films, the gas sorption capacity is low due to the low free volume. Thus, the amount of N_2 sorption is below the detection limit of the instrument and not reported here. It can be noticed that higher oligo (EO) content in the membrane leads to increased CO_2 solubility. Compared with XLPDMSPNB membranes, the incorporation of oligo (EO) moiety contributed to about 30% increase of CO_2 solubility. In Table 2, the k_D value generally increases with oligo (EO) incorporation, providing solid support that the incorporation of CO_2-philic oligo (EO) groups

contribute to higher CO_2 dissolution into the polymer matrix. The decrease of C'_H (which reflects the sorption by FFV) parameter is likely due to the higher membrane density, which leads to the slight drop of FFV. Although the N_2 sorption cannot be measured, we expect that the decrease of C'_H value with more oligo (EO) in the polymer matrix should reduce the N_2 Langmuir sorption, and the non N_2-philic oligo (EO) moiety cannot compensate the solubility by increasing k_D value. Thus, the lower N_2 sorption should result in the enhancement of overall CO_2/N_2 solubility selectivity. However, after 34% oligo (EO) amount is reached, no further change of selectivity is observed with the increase of oligo (EO) content. Feng *et al* and Reijerkerk *et al* also reported the plateauing behavior of CO_2/N_2 selectivity with high PEO content in their studies.[16, 46] Based on their explanation and the gas separation performance of our membranes, we expect that when oligo (EO) composition is lower than 34%, the gas selectivity is predominantly influenced by solubility selectivity. After the oligo (EO) incorporation of 34% is reached, the CO_2 solubility becomes saturated, which is likely due to the plasticization effect that become considerable within membrane matrix, leading to no further change of gas selectivity with more oligo (EO) content.

Based on the gas transport property, the newly-designed oligo (EO)-PDMSPNB membranes provide solid evidence that the combination of fast PDMSPNB dynamics and strong oligo (EO)-CO_2 interaction contribute to an enhanced performance compared to both PDMS and oligo (EO). More fundamental studies will be performed to further disentangle the complex interaction between polymer and gas molecules on the surface and in the bulk.

3. Conclusion

In conclusion, we have synthesized oligo (EO)-PDMSPNB membranes by using an *in-situ* ROMP technique. All prepared membranes exhibit significantly higher CO_2 permeability than previously reported PEO-containing membranes. The highest performing membrane with 34% oligo (EO) content, exhibiting CO_2 permeability ~3400 Barrer and CO_2/N_2 selectivity

~19, has achieved performance very close to the Robeson upper bound, and its highly permeable nature could potentially benefit practical flue gas separation. The oligo (EO) content was found to significantly influence gas separation performance, which has been attributed to controlling CO_2 solubility within the copolymer matrix. Furthermore, these results demonstrate that by carefully tuning the oligo (EO)/PDMS composition, it is possible to significantly increase CO_2/N_2 selectivity with a small loss in permeability. The versatility of the ROMP technique allows us to incorporate various CO_2-philic groups into the PDMS matrix, providing tunable gas separation performance for future development. These findings provide strong support to practical CO_2 separation material development, as well as fostering fundamental understanding of the gas separation process using polymer membranes.

4. Experimental Section

Materials: (Bicycloheptenyl) ethyl terminated polydimethylsiloxane (PDMSNB) with a weight-average molecular weight range from 12,000-16,000 g/mol was purchased from Gelest Inc. trans-5-Norbornene-2,3-dicarbonyl chloride (NB-COCl), Poly(ethylene glycol) methyl ether (oligo (EO)), Pyridine, 4-(Dimethylamino)pyridine (DMAP), Grubbs catalyst, 2nd generation (Grubbs-II), Tetrahydrofuran (THF) and anhydrous dichloromethane (DCM) were purchased from Sigma-Aldrich. Nitrogen and carbon dioxide gas cylinders (99.99% purity) were obtained from Air Liquide. All ^{1}H and ^{13}C NMR spectra were collected using a Bruker ADVANCE III spectrometer operating at 400 MHz for ^{1}H and 100 MHz for ^{13}C. Chemical shifts were reported in ppm downfield from tertamethylsilane. $CDCl_3$ (deuterated chloroform) was used as the solvent for all NMR samples.

Synthesis of norbornene- oligo (ethylene oxide) (NB- oligo (EO)): The NB-oligo (EO) monomers were prepared by adding 2.5 equivalents of pyridine (45.65 mmol, 3.68 mL) *via*

syringe into a flask equipped with 1 equivalent (18.26 mmol) NB-COCl, 0.05 equivalent (0.913 mmol) DMAP, 2 equivalents (36.52 mmol) oligo (EO), and 100 mL dry THF cooled in an ice bath. The reaction was stirred under argon for 72h at 40 °C. The pyridine salts were filtered out and remaining pyridine was removed by rotary evaporation as an azeotrope with n-heptane. The yield of the reaction was in 80%-90% range, all monomers are yellow to orange viscous liquids. ^{1}H NMR ($CDCl_3$, 400 MHz): 6.24 ppm (bs, 1H, CH=CH), 6.04 (bs, 1H, CH=CH), 4.30-4.10 (m, 4H, $C=O(O)CH_2$), 3.79-3.56 (m, 8H, CH_2OCH_2), 3.52 (m, 4H, CH_2OCH_3), 3.40 (t, 1H, nb), 3.35 (bs, 6H, OCH_3), 3.26 (bs, 1H, nb), 3.12 (bs, 1H, nb), 2.71 (d, 1H, nb), 1.59 (d, 1H, nb), 1.42 (d, 1H, nb).

Oligo (EO)-PDMSPNB membrane fabrication: The oligo (EO)-PDMSPNB membranes were synthesized *via* the *in-situ* ring-opening metathesis polymerization (ROMP) of PDMSNB and NB-oligo (EO) (Scheme 1). In a typical process, PDMSNB (300 mg, 2.14×10^{-5} mol) and NB-oligo (EO) (200 mg, 3.07×10^{-4} mol) were dissolved in DCM (6 mL). In a separate vial, Grubbs-II catalyst (10 mg, 1.18×10^{-5} mol) was dissolved in DCM (2 mL). Then 1 mL of the Grubbs-II catalyst stock solution was added to the monomer solution and shaken for 60 s before being poured into a 100 mL PTFE dish (with a diameter of 10 cm). The PTFE dish was covered with aluminum foil for 24 h in which the *in-situ* cross-linked membrane was formed. A mixture of ethyl vinyl ether (2 mL) in DCM (6 mL) was added to the film to terminate the metathesis reaction. The membrane was dried under argon atmosphere overnight and moved to a vacuum oven for 3 days to remove residual solvent. Finally, the cross-linked free-standing polymer membrane was detached from the PTFE dish and cut into pieces for further testing. Membranes with NB-oligo (EO) feed ratio ranged from 20 wt% to 50 wt% were synthesized. The membrane thickness ranged from 140-170 μm.

Fourier transform infrared spectroscopy (FT-IR): FT-IR was conducted using a Nicolet iS50 FT-IR spectrometer equipped with a deuterated triglycine sulfate (DTGS) detector. A

minimum of 128 scans were signal-averaged to obtain the final spectrum. An open-air measurement was used for the background.

Dynamic Mechanical Analysis (DMA): DMA tests were performed using a TA Q800 Instrument. Films were cut into approximately (6.0 × 5.0 × 0.1) mm specimens for tensile tests. All samples were elongated until failure/break with a constant strain rate (10%/min) at 25 ^{o}C. The modulus was determined using the 1% secant method to the minimize error.

Differential scanning calorimetry (DSC): Differential scanning calorimetry (DSC) measurements were performed under argon atmosphere using a TA Instruments Q1000 with aluminum hermetic pans. Temperature-modulated DSC (TMDSC) measurements were performed using the following procedure: sample was equilibrated at 120 °C, isothermal for 10 min to erase the thermal history, and then cooled to −160 °C at 3 °C/min with a modulation of ±1 °C/min, and then heated to 120 °C. The glass transition temperature (T_g) value was taken as the midpoint of the transition step in the heating process of the reversible heat flow signals.

Thermogravimetric Analysis (TGA): The thermal stability of the oligo (EO)-PDMSPNB membranes was examined using a TA Instruments Q-50 TGA. About 10 mg sample was placed in the platinum pan and equilibrated at room temperature. TGA measurements were conducted from room temperature to 800 °C under a nitrogen atmosphere at a rate of 20 K/min.

Gas permeability measurements: The permeation measurements were performed at room temperature with single gas tests using a custom test chamber following the constant-volume variable-pressure method under 5 different pressures: 0.2, 0.5, 1.0, 1.5 and 2.0 atm. Before loading, the membrane sample was mounted using a 47 mm non-porous aluminum tape disc with a hole (10 mm diameter) cut in the center and sealed with epoxy (Devcon). The mounted

membrane sample was then placed on a highly porous stainless-steel support, which was for mechanical stability and shows negligible resistance to gases, and the entire assembly was installed into the test chamber. The chamber was evacuated with a mechanical pump to a base pressure of 20 mTorr. The membrane was allowed to remain in the test chamber overnight to fully degas the solvent residue and reach a steady base pressure. All permeability data are based on duplicate measurements on two different samples and the average value was reported.

Gas solubility measurement: Low-pressure CO_2 solubility measurements were acquired using an Intelligent Gravimetric Analyzer (Hiden Analytical Limited, UK). In a typical experiment, approximately 50 mg of a particular membrane sample was loaded into a quartz container and evacuated to 0.003 bar for 6 h at 150 °C to degas and dry the sample. All measurements were performed at room temperature. The mass uptake (corrected for buoyancy) was then measured as a function of pressure up to a final pressure of 1 atm to obtain the absorption isotherm. Desorption isotherms were subsequently acquired by measuring the mass as a function of decreasing pressure to ensure that the solubility behavior was reversible and to test for the hysteresis effects.

Supporting Information

Supporting Information is available from the Wiley Online Library or from the author.

Acknowledgements

The initial study was sponsored by the Laboratory Directed Research and Development Program of Oak Ridge National Laboratory, managed by UT-Battelle, LLC, for the U.S. Department of Energy. Follow on research is sponsored by U.S. Department of Energy, Office of Fossil Energy, Carbon Capture Program and by the Oak Ridge National Laboratory

Technology Innovation Program using technology transfer license royalties. Oak Ridge National Laboratory is managed by UT-Battelle, LLC, for the U. S. Department of Energy under Contract No. DE-AC05-00OR22725. JM acknowledges partial financial support on polymer and monomer synthesis and JMC acknowledges partial financial support on computational simulation by the U.S. Department of Energy, Office of Science, Basic Energy Sciences, Materials Sciences and Engineering Division. BKL acknowledges financial support from the UTK/ORNL Science Alliance JDRD program.

Received: ((will be filled in by the editorial staff))
Revised: ((will be filled in by the editorial staff))
Published online: ((will be filled in by the editorial staff))

References

[1] I. Capellán-Pérez, I. Arto, J. M. Polanco-Martínez, M. González-Eguino, M. B. Neumann, *Energy Environ. Sci.* **2016**, *9*, 2482-2496.
[2] B. Metz, O. Davidson, H. De Coninck, M. Loos, L. Meyer, Intergovernmental Panel on Climate Change, Geneva (Switzerland). Working Group III, 2005.
[3] R. K. Pachauri, M. R. Allen, V. R. Barros, J. Broome, W. Cramer, R. Christ, J. A. Church, L. Clarke, Q. Dahe, P. Dasgupta, *Climate change 2014: synthesis report. Contribution of Working Groups I, II and III to the fifth assessment report of the Intergovernmental Panel on Climate Change*, IPCC, **2014**.
[4] D. S. Sholl, R. P. Lively, *Nature* **2016**, *532*, 435-437.
[5] P. Angelini, T. Armstrong, R. Counce, W. Griffith, T. LKlasson, G. Muralidharan, C. Narula, V. Sikka, G. Closset, G. Keller, *DOE, EERE Office, Washington, DC* **2005**, 103.
[6] L. M. Robeson, *J. Membr. Sci.* **1991**, *62*, 165-185.
[7] L. M. Robeson, *J. Membr. Sci.* **2008**, *320*, 390-400.
[8] T. C. Merkel, H. Lin, X. Wei, R. Baker, *J. Membr. Sci.* **2010**, *359*, 126-139.
[9] H. B. Park, J. Kamcev, L. M. Robeson, M. Elimelech, B. D. Freeman, *Science* **2017**, *356*, eaab0530.
[10] B. D. Freeman, *Macromolecules* **1999**, *32*, 375-380.
[11] S. L. Liu, L. Shao, M. L. Chua, C. H. Lau, H. Wang, S. Quan, *Prog. Polym. Sci.* **2013**, *38*, 1089-1120.
[12] B. Yu, H. Cong, Z. Li, J. Tang, X. S. Zhao, *J. Appl. Polym. Sci.* **2013**, *130*, 2867-2876.
[13] A. Car, C. Stropnik, W. Yave, K.-V. Peinemann, *Sep. Purif. Technol.* **2008**, *62*, 110-117.
[14] V. Bondar, B. Freeman, I. Pinnau, *J. Polym. Sci., Part B: Polym. Phys.* **1999**, *37*, 2463-2475.
[15] W. Yave, A. Car, S. S. Funari, S. P. Nunes, K.-V. Peinemann, *Macromolecules* **2009**, *43*, 326-333.
[16] S. Feng, J. Ren, K. Hua, H. Li, X. Ren, M. Deng, *Sep. Purif. Technol.* **2013**, *116*, 25-34.
[17] S. J. Kim, H. Jeon, D. J. Kim, J. H. Kim, *ChemSusChem* **2015**, *8*, 3783-3792.
[18] H. Lin, B. D. Freeman, *J. Membr. Sci.* **2004**, *239*, 105-117.
[19] D. Gomes, S. P. Nunes, K.-V. Peinemann, *J. Membr. Sci.* **2005**, *246*, 13-25.
[20] Y. Ichiraku, S. Stern, T. Nakagawa, *J. Membr. Sci.* **1987**, *34*, 5-18.
[21] K. Nagai, T. Masuda, T. Nakagawa, B. D. Freeman, I. Pinnau, *Prog. Polym. Sci.* **2001**, *26*, 721-798.

[22] H. Feng, T. Hong, S. M. Mahurin, K. D. Vogiatzis, K. R. Gmernicki, B. K. Long, J. W. Mays, A. P. Sokolov, N.-G. Kang, T. Saito, *Polymer Chemistry* **2017**, *8*, 3341-3350.
[23] P. M. Budd, K. J. Msayib, C. E. Tattershall, B. S. Ghanem, K. J. Reynolds, N. B. McKeown, D. Fritsch, *J. Membr. Sci.* **2005**, *251*, 263-269.
[24] P. M. Budd, N. B. McKeown, B. S. Ghanem, K. J. Msayib, D. Fritsch, L. Starannikova, N. Belov, O. Sanfirova, Y. Yampolskii, V. Shantarovich, *J. Membr. Sci.* **2008**, *325*, 851-860.
[25] P. M. Budd, N. B. McKeown, *Polymer Chemistry* **2010**, *1*, 63-68.
[26] J. Ahn, W.-J. Chung, I. Pinnau, J. Song, N. Du, G. P. Robertson, M. D. Guiver, *J. Membr. Sci.* **2010**, *346*, 280-287.
[27] T. Merkel, V. Bondar, K. Nagai, B. Freeman, I. Pinnau, *J. Polym. Sci., Part B: Polym. Phys.* **2000**, *38*, 415-434.
[28] T. Hong, Z. Niu, X. Hu, K. Gmernicki, S. Cheng, F. Fan, J. C. Johnson, E. Hong, S. Mahurin, D. e. Jiang, *ChemSusChem* **2015**, *8*, 3595-3604.
[29] S. Wang, X. Li, H. Wu, Z. Tian, Q. Xin, G. He, D. Peng, S. Chen, Y. Yin, Z. Jiang, *Energy Environ. Sci.* **2016**, *9*, 1863-1890.
[30] T. Khosravi, M. Omidkhah, *RSC Advances* **2015**, *5*, 12849-12859.
[31] V. A. Kusuma, B. D. Freeman, S. L. Smith, A. L. Heilman, D. S. Kalika, *J. Membr. Sci.* **2010**, *359*, 25-36.
[32] Z. Tian, T. Saito, D.-e. Jiang, *The Journal of Physical Chemistry A* **2015**, *119*, 3848-3852.
[33] T. Hong, S. Chatterjee, S. M. Mahurin, F. Fan, Z. Tian, D.-e. Jiang, B. K. Long, J. W. Mays, A. P. Sokolov, T. Saito, *J. Membr. Sci.* **2017**, *530*, 213-219.
[34] A. Abdelghany, E. Abdelrazek, S. Badr, M. Morsi, *Materials & Design* **2016**, *97*, 532-543.
[35] S. Chapi, S. Raghu, H. Devendrappa, *Ionics* **2015**, 1-12.
[36] K. Kumar, M. Ravi, Y. Pavani, S. Bhavani, A. Sharma, N. R. VVR, *J. Non-Cryst. Solids* **2012**, *358*, 3205-3211.
[37] D. Bodas, C. Khan-Malek, *Microelectron. Eng.* **2006**, *83*, 1277-1279.
[38] D. W. Grainger, T. Okano, S. W. Kim, D. G. Castner, B. D. Ratner, D. Briggs, Y. Sung, *J. Biomed. Mater. Res.* **1990**, *24*, 547-571.
[39] G. Çakmak, Z. Küçükyavuz, S. Küçükyavuz, H. Çakmak, *Composites Part A: Applied Science and Manufacturing* **2004**, *35*, 417-421.
[40] M. Ochsner, M. R. Dusseiller, H. M. Grandin, S. Luna-Morris, M. Textor, V. Vogel, M. L. Smith, *LChip* **2007**, *7*, 1074-1077.
[41] K. M. Choi, J. A. Rogers, *J. Am. Chem. Soc.* **2003**, *125*, 4060-4061.
[42] X. He, J. Widmaier, J. Herz, G. Meyer, *Poly* **1992**, *33*, 866-871.
[43] M. Srividhya, B. Reddy, *J. Polym. Sci., Part A: Polym. Chem.* **2007**, *45*, 1707-1726.
[44] F. T. Simon, J. Rutherford Jr, *J. Appl. Phys.* **1964**, *35*, 82-86.
[45] W. J. Koros, A. Chan, D. Paul, *J. Membr. Sci.* **1977**, *2*, 165-190.
[46] S. R. Reijerkerk, M. H. Knoef, K. Nijmeijer, M. Wessling, *J. Membr. Sci.* **2010**, *352*, 126-135.

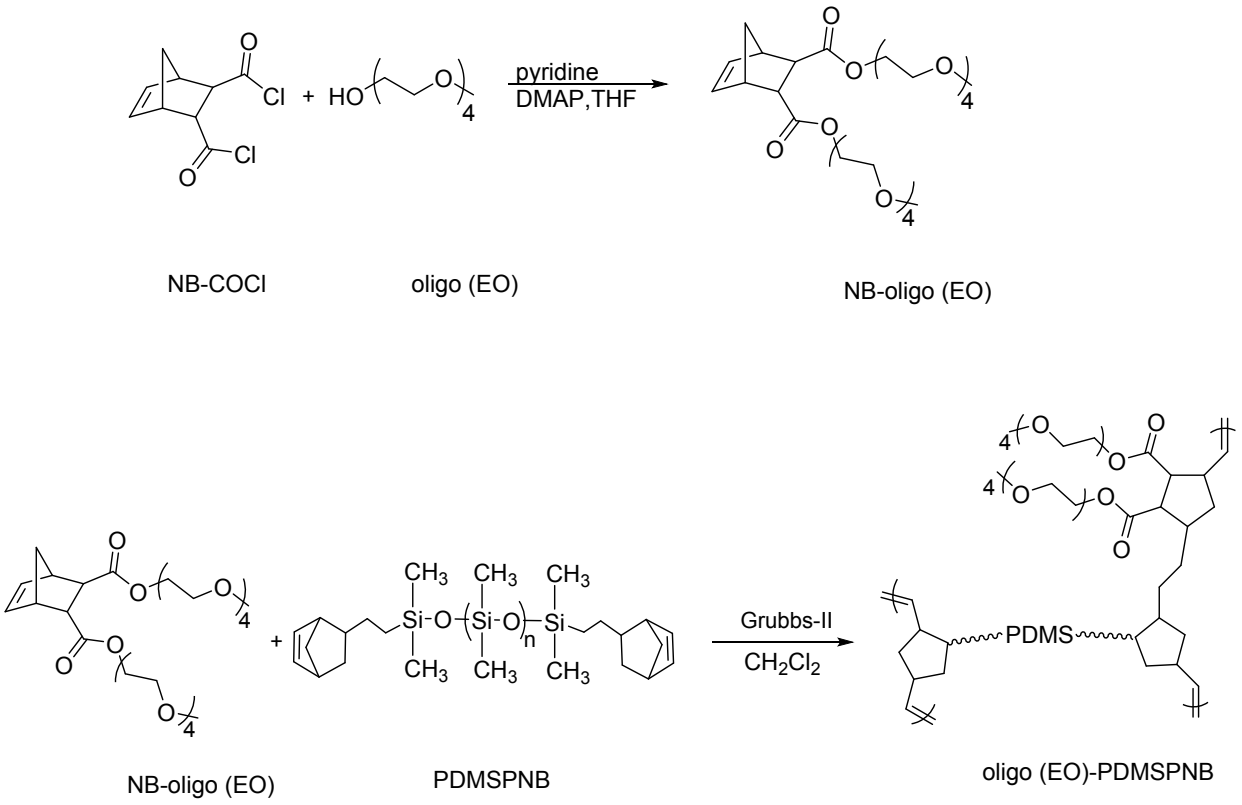

Scheme 1. Synthesis of NB-oligo (EO) and ROMP reaction of the oligo (EO)-co-PDMSPNB membranes.

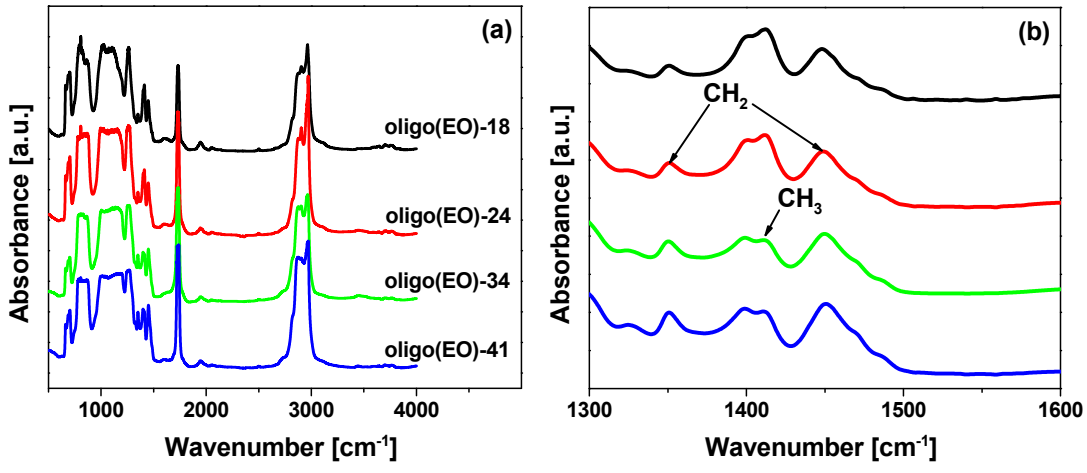

Figure 1. (a) FTIR spectra of oligo (EO)-PDMSPNB membranes and (b) zoomed in spectra (1300 cm^{-1} to 1600 cm^{-1}) demonstrating the systematical change of CH_2 scissoring and CH_2 asymmetric bending peaks of oligo (EO) and CH_3 asymmetric deformation peaks of PDMS.

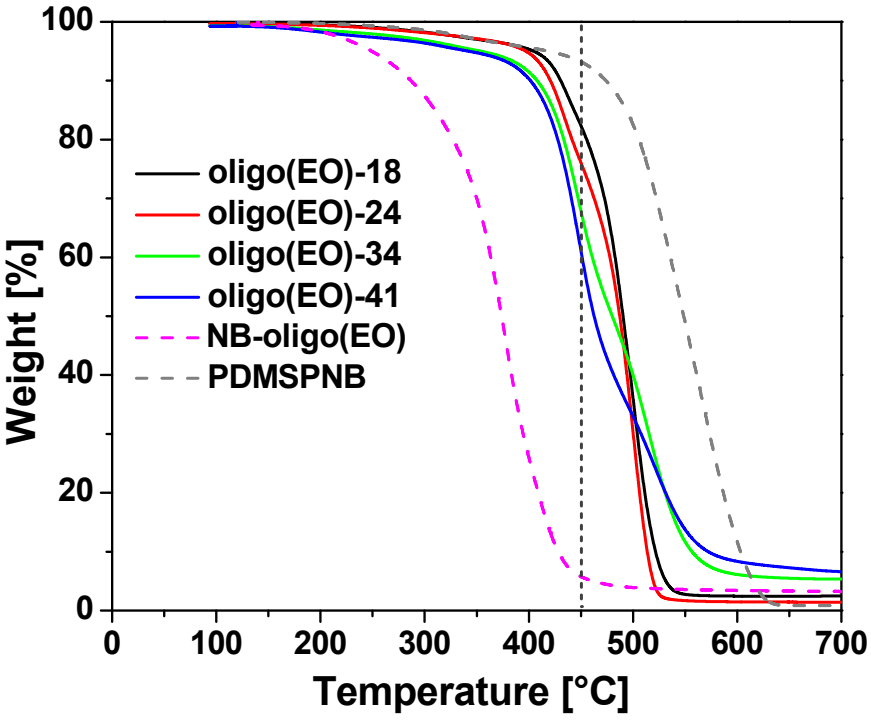

Figure 2. TGA curves of oligo (EO)-PDMSPNB membranes. Data of NB-oligo (EO) and pure XLPDMSPNB membranes are shown in dashed curves. Vertical dashed line indicates the onset temperature of PDMS decomposition.

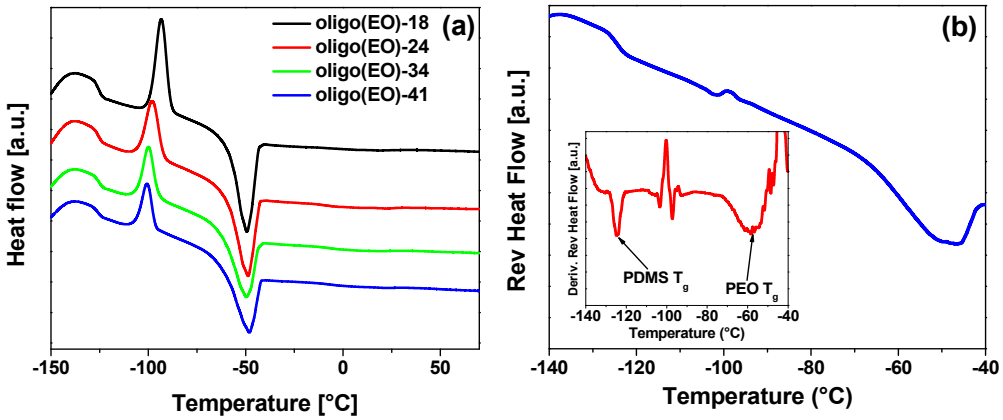

Figure 3. (a) DSC curves for oligo (EO)-PDMSPNB membranes. All curves have been shifted vertically to illustrate the systematic change of the peak shape and position. (b) Reversible heat flow curve of oligo (EO)-41 membrane. Inset is the derivative of reversible heat flow change. The T_g is determined from both the transition process in reversible heat flow curves and the peak position in the derivative curves.

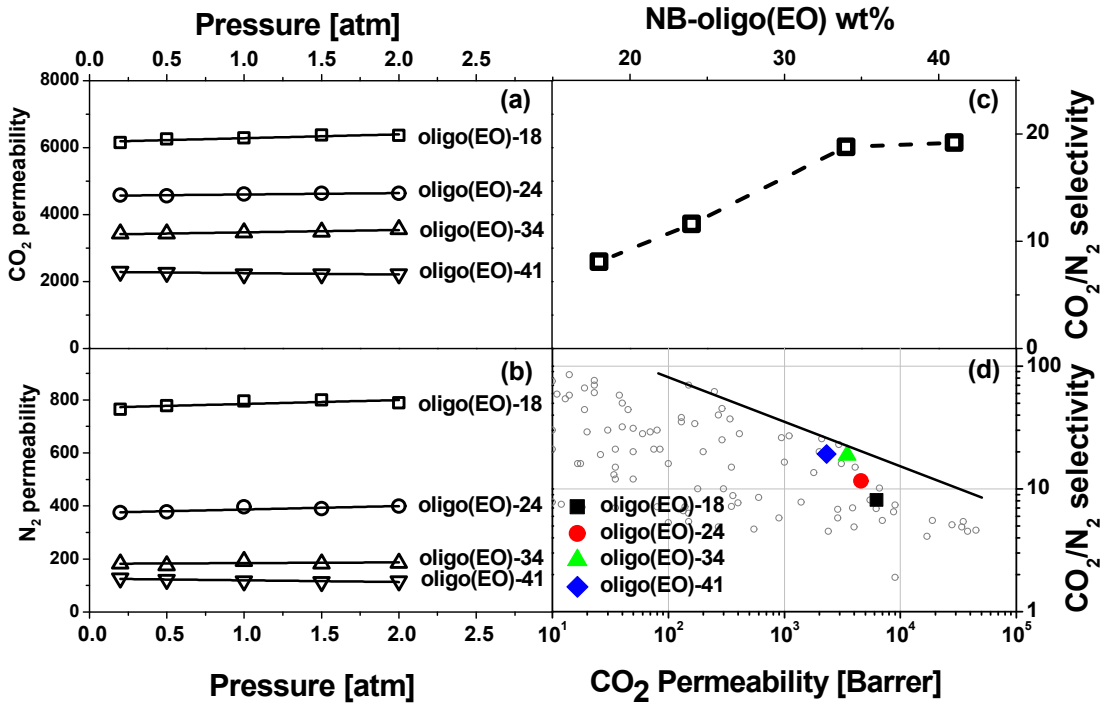

Figure 4. (a) CO_2 permeability, (b) N_2 permeability, (c) CO_2/N_2 selectivity for PEO-PDMSPNB membranes, and (d) Summary of the oligo (EO)-PDMSPNB membranes as a function of oligo (EO) content in a Robeson plot.

Table 1. Summary of density, membrane composition, glass transition temperature and gas transport properties for oligo (EO)-PDMSPNB samples.

Sample[a)]	Density (g/cm^3)	$T_{g,1}$ (°C)	$T_{g,2}$ (°C)	P_0 [Barrer]		CO_2/N_2 selectivity	m [b)]×10^3 [1/atm]	
				CO_2	N_2		CO_2	N_2
XLPDMSPNB[28]	0.98	-125	-	6700	490	13.8	-	
oligo (EO)-18	0.98	-124	-53	6200 ± 70	770 ± 10	8.1 ± 0.2	18.5 ± 0.1	19.0 ± 0.3
oligo (EO)-24	1.01	-124	-54	4600 ± 60	370 ± 10	12.4 ± 0.2	9.0 ± 0.1	28.6 ± 0.5
oligo (EO)-34	1.04	-124	-57	3400 ± 20	180 ± 10	18.8 ± 0.4	20.9 ± 0.1	15.0 ± 0.8
oligo (EO)-41	1.06	-124	-58	2300 ± 30	120 ± 5	19.2 ± 0.5	-17.4 ± 0.1	-20.1 ± 1.3

[a)] NB-oligo (EO) wt% determined by TGA measurements; [b)] slope of pressure dependence of permeability

Table 2. Summary of dual-mode model parameters and CO_2 solubility for oligo (EO)-PDMSPNB membranes.

Sample code	k_D $\left[\frac{cm^3(STP)}{cm^3\ atm}\right]$	C'_H $\left[\frac{cm^3(STP)}{cm^3}\right]$	b $[atm^{-1}]$	S $\left[\frac{cm^3(STP)}{cm^3\ atm}\right]$
oligo (EO)-18	0.78	4.55	0.1	1.16
oligo (EO)-24	0.91	3.50	0.1	1.20
oligo (EO)-34	1.06	2.44	0.1	1.26
oligo (EO)-41	1.07	2.32	0.1	1.27
XLPDMSPNB[28]	-	-	-	0.9-1.0

The table of contents entry:

A series of cross-linked oligo (ethylene oxide)-co-(polydimethylsiloxane-norbornene) membranes with varied composition is synthesized. These membranes show remarkably high CO_2 permeabilities (3400 Barrer) and their separation performance approaches the Robeson Upper Bound. The gas transport properties are found to be directly proportional to oligo (EO) content incorporation, which stems from the increased solubility selectivity change within the copolymer matrix.

Keyword: membrane gas separation, CO_2-philic, oligo (ethylene oxide), polydimethylsiloxane, high permeability

*Tao Hong, Sophia Lai, Shannon M. Mahurin, Peng-Fei Cao, Dmitry N. Voylov, Harry M. Meyer, III, Christopher B. Jacobs, Jan-Michael Y. Carrillo, Alexander Kisliuk, Ilia N. Ivanov, De-en Jiang, Brian K. Long, Jimmy W. Mays, Alexei P. Sokolov, Tomonori Saito**

Title: Highly-permeable Oligo (ethylene oxide)-co-Poly(dimethylsiloxane) Membranes for Carbon Dioxide Separation

ToC figure

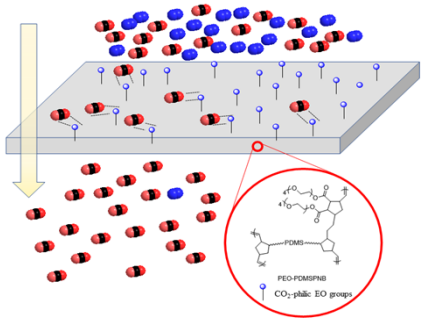

Supporting Information

Highly-permeable Oligo (ethylene oxide)-co-Poly(dimethylsiloxane) Membranes for Carbon Dioxide Separation

*Tao Hong, Sophia Lai, Shannon M. Mahurin, Peng-Fei Cao, Dmitry N. Voylov, Harry M. Meyer, III, Christopher B. Jacobs, Jan-Michael Y. Carrillo, Alexander Kisliuk, Ilia N. Ivanov, De-en Jiang, Brian K. Long, Jimmy W. Mays, Alexei P. Sokolov, Tomonori Saito**

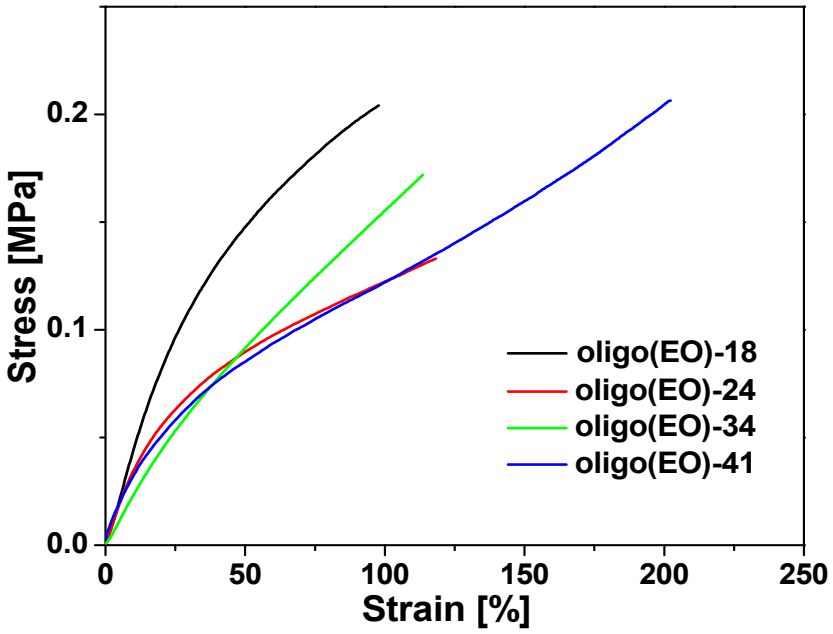

Figure S1. Tensile properties of oligo (EO)-PDMSPNB membranes.

Table S1. Tensile test data for PEO-PDMSPNB membranes.

Sample	Young's modulus Et(MPa)	Ultimate tensile strength (MPa)	Elongation at break ε (%)
oligo (EO)-18	0.21	0.20	97.9
oligo (EO)-24	0.39	0.13	118.2
oligo (EO)-34	0.14	0.17	113.6
oligo (EO)-41	0.37	0.21	202.3

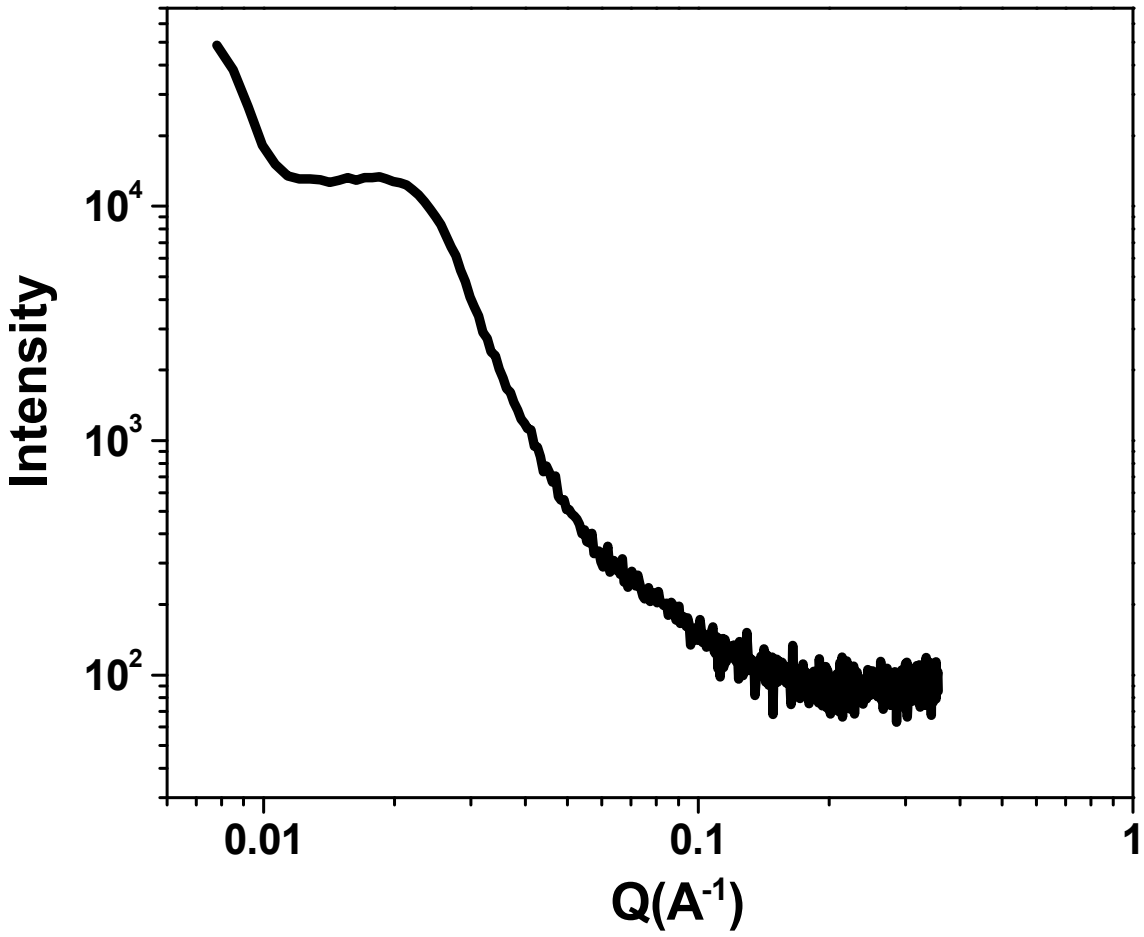

Figure S2. SAXS profile of the oligo (EO)-41 membrane.

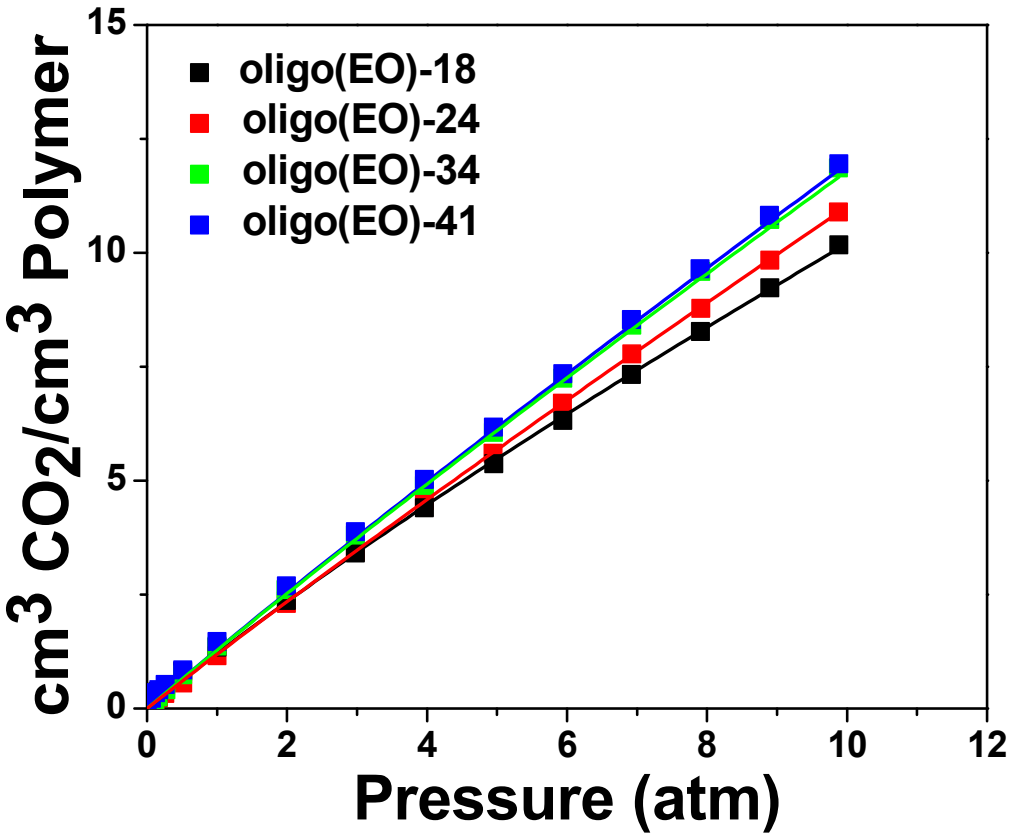

Figure S3. CO_2 sorption isotherms for oligo (EO)-PDMSPNB membranes. The solid curves show the fits to the dual-mode sorption model.